Comprehensive Model of the Degradation of Organic Light-Emitting Diodes and Application for Efficient, Stable Blue Phosphorescent Devices with Reduced Influence of Polarons

Bomi Sim,[1] Jong Soo Kim,[2] Hyejin Bae,[2] Sungho Nam,[2] Eunsuk Kwon,[2] Ji Whan Kim,[2] Hwa-Young Cho,[2] Sunghan Kim,[2,†] and Jang-Joo Kim[1,3,*]

[1] *Department of Materials Science and Engineering, Seoul National University, Seoul 151-744, South Korea*
[2] *Samsung Advanced Institute of Technology, SEC, 130 Samsung-ro, Yeongtong-gu, Suwon-si, Gyeonggi-do, 443-803, Korea*
[3] *Research Institute of Advanced Materials (RIAM), Seoul National University, Seoul 151-744, South Korea*

(Received 11 December 2019; revised 21 May 2020; accepted 2 June 2020; published 3 August 2020)

We present a comprehensive model to analyze quantitatively and predict the process of degradation of organic light-emitting diodes (OLEDs) considering all possible degradation mechanisms, i.e., polarons, excitons, exciton-polaron interactions, exciton-exciton interactions, and impurity effects. The loss of efficiency during degradation is presented as a function of quencher density. The density and generation mechanisms of quenchers are extracted using a voltage-rise model. The comprehensive model is applied to stable blue phosphorescent OLEDs, and the results show that the model describes the voltage rise and external-quantum-efficiency loss very well, and that the quenchers in the emitting layer (EML) are generated mainly by polaron-induced degradation of dopants. Quencher formation is confirmed by mass spectrometry. The polaron density per dopant molecule in the EML is reduced by controlling the emitter doping ratio, resulting in the highest reported lifetime LT_{50} of 431 h for an initial brightness of 500 cd/m^2 with a commission internationale de l'éclairage y coordinate less than 0.25, and a high external quantum efficiency greater than 18%.

DOI: 10.1103/PhysRevApplied.14.024002

I. INTRODUCTION

Organic light-emitting diodes (OLEDs) are widely used in displays in cellular phones and TVs, and their application is being extended to lighting. The efficiency of blue OLEDs in these devices is still low compared with phosphorescent red and green OLEDs [1–4], and the device lifetimes of triplet-harvesting phosphorescent and TADF (thermally activated delayed fluorescent) blue OLEDs are too short for them to be used in real displays [5–11]. The development of highly efficient pure blue OLEDs with long lifetimes is a key research topic.

The degradation processes of OLEDs are quite complicated. However, with improved encapsulation and developments in materials and purity, extrinsic sources of degradation have been mostly eliminated. Intrinsic degradation has also been largely reduced in red and green phosphorescent OLEDs and blue fluorescent OLEDs to a level sufficient for practical use, but not in blue phosphorescent and TADF OLEDs. Various mechanisms, such as exciton-exciton [8] or exciton-polaron interactions [6,12,13], excitons themselves [13–15], and radical-ion pairs between host excitons and dopants [9], have been proposed to explain the *intrinsic* degradation of (blue) OLEDs. Quencher generation mechanisms have been reported based on interactions between molecules (excitons and/or polarons) in which an unstable (weak) molecule, either in a neutral or in a charged state (polaron), is dissociated by a highly excited state (hot exciton) with sufficient energy, formed by energy transfer [6,8,9,11]. A few degradation models for OLEDs have also been proposed. Giebink *et al.* reported a model of luminance loss and voltage rise in blue phosphorescent OLEDs (PhOLEDs) and proposed exciton-polaron annihilation as the primary mechanism of defect formation [6]. Schmidt *et al.* and Holmes's group presented luminance-loss models that describe the relative ratio of exciton formation efficiency and effective quantum efficiency during the degradation of green PhOLEDs [16–18]. A model describing the degradation processes in polymer LEDs has also been reported [19].

As quencher formation is likely to be caused by various factors simultaneously, it is necessary to consider a combination of the previously proposed mechanisms. To

*jjkim@snu.ac.kr
†shan0819.kim@samsung.com

develop a general degradation model, it is necessary to include additional factors that may contribute to quencher formation, such as unstable polaron states not involving excitons, and inevitable minute amounts of impurities incorporated during device fabrication (O_2, H_2O, or other volatile components), which depend on the vacuum level for small molecules and on solvent incorporation for polymers. Despite the potential instability and high density of polaron states in the emitting layer (EML) during operation, the presence of polarons in the EML has not been reported as a major reason for degradation. In addition, rapid changes in driving voltage and luminance over a short time scale can be caused by impurities, such as water and oxygen [5,7]. However, conventional degradation models do not consider impurity factors. Therefore, a model that can describe the quantitative contribution of each mechanism to degradation and explain more general and comprehensive degradation phenomena, including quencher formation, is still needed.

Here, we present a comprehensive and general model for describing the *intrinsic* degradation of OLEDs along with the effect of the inevitable minute amounts of impurities described above. Our model consists of two equations, describing the efficiency loss and the voltage increase during electrical operation as functions of the quencher density. The effects of the quenchers on the exciton formation efficiency and the effective quantum efficiency are described in the equations by measurable parameters. Polaron and impurity effects as well as exciton, exciton-polaron, and exciton-exciton interactions are considered to be the mechanisms underlying quencher generation (or degradation). This model allows quantitative analysis of the contribution of each mechanism to the total device degradation. Analysis of a stable blue phosphorescent device using the degradation model shows that quenchers are generated by all such mechanisms, originating from impurities, polarons, excitons, exciton-polaron interactions, and exciton-exciton interactions. The transporting materials are degraded by exciton-mediated processes. Interestingly, however, quenchers in the EML are mainly generated by polaron-induced degradation of dopants. Polarons themselves can have the greatest impact on the degradation of phosphorescent dyes in the EML. In contrast, the transporting materials are degraded by exciton-mediated processes. We then reduce the polaron density per dopant molecule by increasing the emitter doping concentration to achieve the highest reported lifetime LT_{50} (where LT_x is the operation time at which the luminance decreases to x% of its initial value) for a blue phosphorescent device with a commission internationale de l'éclairage (CIE) y coordinate less than 0.25, with a value of 431 h, for an initial brightness of 500 cd/m^2 while maintaining a high external quantum efficiency (EQE) of around 18%.

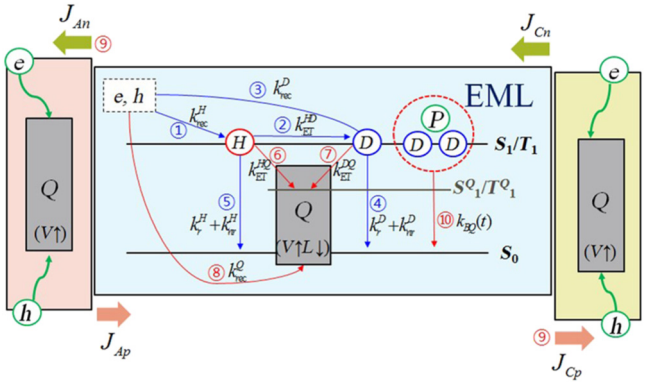

FIG. 1. Schematic diagram of exciton generation and annihilation processes. 1, charge recombination in host. 2, energy transfer from host excitons to dopants. 3, charge recombination at dopants. 4, radiative and nonradiative decay of dopant excitons. 5, radiative and nonradiative decay of host excitons. 6, energy transfer from host excitons to quenchers. 7, energy transfer from dopant excitons to quenchers. 8, charge recombination at quenchers. 9, charge leakage from EML. 10, biparticle interactions of dopant excitons.

II. MODEL

A. Modeling of degradation process

The processes of exciton generation and annihilation in an OLED are schematically illustrated in Fig. 1. The sky-blue region represents the EML, while the yellow and orange colors represent the other layers. The processes in the pristine device are indicated by the blue lines. The injected charges are recombined in the host (H) (1) or at dopants (D) (3) with recombination rates of $k^H_{\rm rec}$ and $k^D_{\rm rec}$, respectively, or in other layers, or leak out from the EML (9). The exciton energy of the host is transferred to the dopants at a rate of $k^{HD}_{\rm ET}$ (2) or emitted as light or heat with a decay rate of k^H_r or $k^H_{\rm nr}$ (5), respectively. The dopant excitons, generated by direct recombination on the dopants or energy transfer from the host, decay radiatively or nonradiatively with a decay rate of k^D_r or $k^D_{\rm nr}$, respectively (4).

The additional processes in an aged (or degraded) device are indicated by red lines. Quenchers, indicated by Q in Fig. 1, are assumed to be generated throughout the electrically degraded device, including the EML. We assume that the singlet-to-triplet ratio (1:3), the radiative decay rates, the energy transfer rate from host excitons to dopants, the absorption coefficient in the EML, the refractive indices, and the Purcell factor are constant during the electrical operation of the OLED. The quenchers can act as deep charge traps, nonradiative-recombination centers, and luminance quenchers depending on their energy and location in the device. The rates of the luminance-loss processes are affected by the density of quenchers in the EML. The host excitons can transfer energy to the quenchers

(6) at a rate $k_{\mathrm{ET}}^{HQ}Q(t)_{\mathrm{EML}}$, which reduces the efficiency of energy transfer to the dopants (η_{ET}^{HD}). Here, $Q(t)_{\mathrm{EML}}$ is the quencher density in the EML. Energy transfer from the dopant excitons to the quenchers (7), at a rate $k_{\mathrm{ET}}^{DQ}Q(t)_{\mathrm{EML}}$, and biparticle interaction (10), with an annihilation rate k_{BQ}^{D}, result in luminance quenching as well as quencher generation. When quenchers act as nonradiative recombination centers, the injected charges can be recombined directly at the quenchers (8), with a recombination rate k_{rec}^{Q}, reducing the efficiency of exciton formation in the EML. Note that bimolecular interactions [20–23] and charge leakage [22,23] can also occur in the pristine device.

B. Modeling of efficiency loss

The EQE, η_{EQE}, of an electrically aged device as shown in Fig. 1 can be expressed as follows:

$$\eta_{\mathrm{EQE}}(t) = \left[\frac{J_{Cn}(t) - J_{An}(t)}{J}\right]\left[\frac{k_{\mathrm{rec}}^{H} + k_{\mathrm{rec}}^{D}}{k_{\mathrm{rec}}^{H} + k_{\mathrm{rec}}^{D} + \frac{e}{\varepsilon\varepsilon_0} f\,\mu_n n Q(t)_{\mathrm{EML}}}\right]\left\{\alpha_{\mathrm{EL}}(t)\left[\frac{k_{\mathrm{ET}}^{HD}}{k_{\mathrm{ET}}^{HD} + Fk_r^H + k_{\mathrm{nr,int}}^{H} + k_{\mathrm{ET}}^{HQ}Q(t)_{\mathrm{EML}}}\right] + [1 - \alpha_{\mathrm{EL}}(t)]\right\} \cdot \left[\frac{Fk_r^D}{Fk_r^D + k_{\mathrm{nr,int}}^{D} + k_{\mathrm{ET}}^{DQ}Q(t)_{\mathrm{EML}} + k_{BQ}(t)}\right]\eta_{\mathrm{out}}(t), \tag{1}$$

where $J_{Cn}(t)$ and $J_{An}(t)$ represent the electron current densities at the cathode and anode sides, respectively, of the EML at operation time t, α_{EL} is the ratio of host excitons to the total number of excitons (host excitons plus dopant excitons) formed in the EML, and F is the Purcell factor, describing enhancement of the spontaneous emission rate in the device [24]. The first and second terms on the right-hand side represent the exciton formation efficiency [$\eta_{\mathrm{EF}}(t)$], considering recombination at quenchers. We consider hole traps in the recombination at quenchers, but electron traps can be included, depending on the device. The third and fourth terms represent the effective quantum efficiency [$q_{\mathrm{eff}}(t)$], which is decreased due to the increased exciton quenching. The general model in Eq. (1) describes the effects of $\eta_{\mathrm{EF}}(t)$ and $q_{\mathrm{eff}}(t)$ on the total EQE loss as a function of $Q(t)_{\mathrm{EML}}$. We apply the model to analyze the degradation process of a blue phosphorescent device and to enhance the operational lifetime. All of the rates in Fig. 1 and Eq. (1) can be determined experimentally, as summarized in Appendix A. Equation (1) can be applied to phosphorescent OLEDs as it is, but it can also be applied to fluorescent (one needs to multiply the EQE by 0.25) or TADF OLEDs with slight modifications.

C. Modeling of voltage rise and quencher density

The changes in operating voltage during electrical operation arise from trapped charges generated both inside and outside the EML. We assume that the charge injection does not change over the operation time, because stable injection has been realized for red and green OLEDs and even blue fluorescent OLEDs by using doped transporting layers or charge-injection layers, and the technique can be applied to other devices under study. Assuming that all the quenchers [$Q(x,t)$] act as deep charge traps so that the occupation probability of charges at quenchers is 1, and that the mobilities of free carriers do not change with time under steady-state operation (but the effective mobility is reduced due to the trapped charge carriers), the voltage rise is represented as [6,8]

$$\Delta V(t) = \frac{e}{\varepsilon\varepsilon_0} Q(t) \int_0^L x g(x)\,dx. \tag{2}$$

Here, ε and ε_0 are the relative dielectric constant of the organic layers and the permittivity of free space, respectively, and L is the thickness of the OLED. The quencher density at position x and time t obeys the relationship $Q(x,t) = Q(t)g(x)$, where $g(x)$ is the normalized quencher distribution function, as shown in Appendix B in detail. As quenchers can be formed by polarons, excitons, exciton-polaron interaction, and exciton-exciton interaction, it is necessary to consider the contributions of all possible mechanisms. In addition, we consider the effect of impurities with an initial concentration $A(x)_0$ in the degradation model; these originate from the source materials or are incorporated during the fabrication process, and include H_2O and O_2. This is necessary because the lifetime of OLEDs is significantly influenced by the purity of the materials and by the fabrication process, e.g., by the vacuum level in evaporation processes or residual solvent in solution processes [5,25,26]. Here, we assume that these impurities form quenchers in the initial stage of operation with first-order kinetics represented by $(A + p \xrightarrow{k_{QF}^{\mathrm{imp}}} Q)$, where A is an impurity, p is a polaron, and k_{QF}^{imp} is the rate constant for quencher formation by impurities, resulting in $Q(x,t)_E = A(x)_0\{1 - \exp[-k_{QF}^{\mathrm{imp}} p(x)t]\}$. Different

kinetic equations can be applied depending on the nature of the impurities. This impurity effect accounts for the rapid increase in driving voltage in the initial stage in our specific example discussed later, and then the quencher density due to impurities becomes constant if the impurities are consumed. Then, the quencher formation rate at position x and time t is represented as

$$\frac{dQ(x,t)}{dt} = k_{QF}^{P} p(x,t) + [k_{QF}^{E} + k_{QF}^{EP} p(x,t)] N(x,t) + k_{QF}^{EE} N(x,t)^2 + k_{QF}^{\mathrm{imp}} p(x,t) A(x,t), \quad (3)$$

where $p(x,t)$ is the polaron density, $N(x,t)$ is the exciton density, and $A(x,t)$ is the impurity density, with an initial value of $A(x)_0$. k_{QF}^{P}, k_{QF}^{E}, k_{QF}^{EP}, and k_{QF}^{EE} are the quencher generation rates due to polarons, excitons, exciton-polaron interactions, and exciton-exciton interactions, respectively. The quencher generation rates due to the different mechanisms can be determined by analyzing the voltage rise over time by combining Eqs. (2) and (3). It should be noted that quencher generation due to excitons and due to exciton-polaron interactions under a constant current show the same first-order reaction kinetics with respect to the exciton density. The details of the application of the equations are presented in Appendix B. The density, location, and generation rate of quenchers can be obtained from a best fit of the voltage-rise model to experimental data, for instance, by using the least-squares method.

III. RESULTS AND DISCUSSION

A. Application to a blue phosphorescent device

Figure 2(a) shows the structure [9,27], with an energy-level diagram, of the blue phosphorescent device used for analysis of the degradation mechanism using the degradation model. A blue-emitting Ir dopant and a wide-band-gap host (mCBP-CN) are used in the EML, with an emitter doping concentration of 10 wt %; their chemical structures are shown in Fig. 2(b). The J-V-L characteristics are shown in Fig. 2(c). The experimentally obtained maximum EQE of the pristine device is 18.3%, as shown in Fig. 2(d), and the CIE coordinates of the emitted light are (0.15, 0.23) at $J = 10$ mA/cm^2 [Fig. 2(e)]. The emission spectra do not change during operation, indicating that the recombination zone does not change over the operation time. The exciton

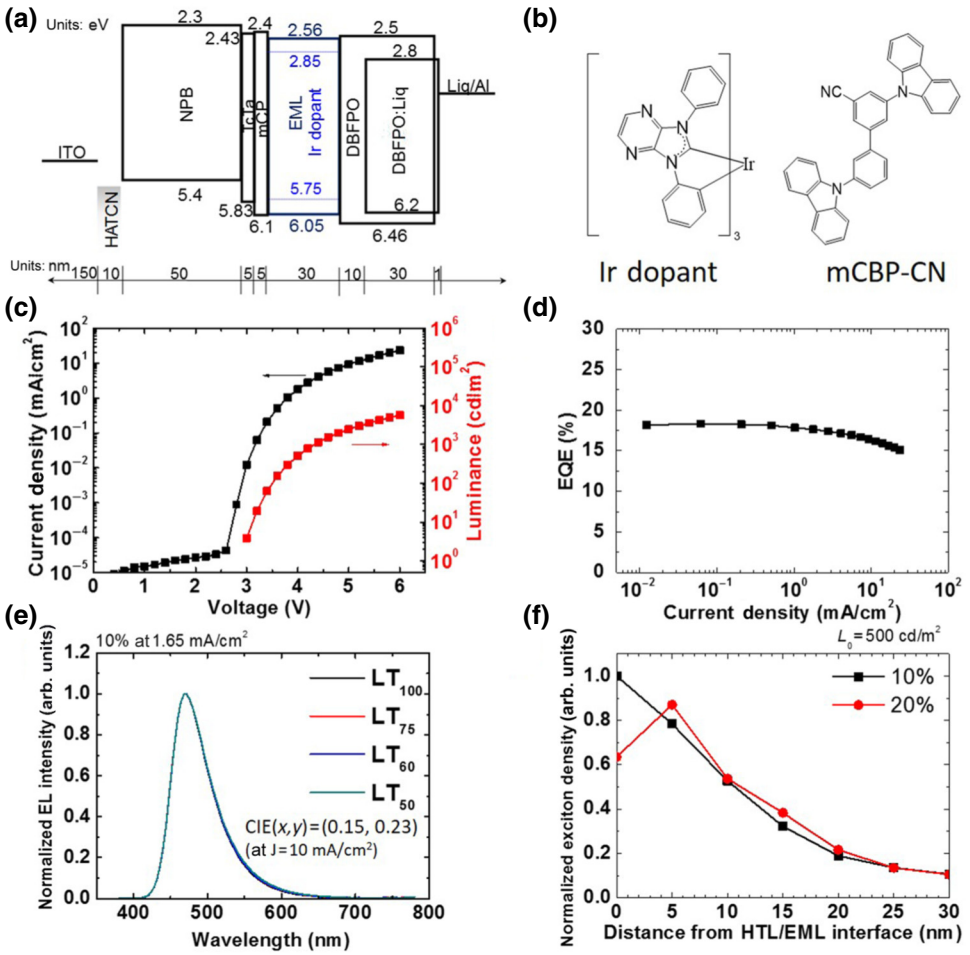

FIG. 2. Electrical characteristics of the blue phosphorescent device used in our model. (a) Schematic device structure, with energy levels (in eV) and thickness diagram. (b) Chemical structures of dopant and host. (c) Current-density–voltage–luminance (J-V-L) characteristics. (d) EQE as a function of current density. (e) Normalized electroluminescence (EL) spectra over time. The emission spectra remain the same during degradation. (f) Exciton profiles at 500 cd/m^2 determined by the sensing-layer method. The doping concentration of the phosphorescent dye in the EML is 10% except for Fig. 2(f). ITO, indium tin oxide; HATCN, 145 8911-hexaazatriphenylenehexacarbonitrile; NPB, *N*,*N*-di(1-naphthyl)-*N*,*N*-diphenyl-(1,1-biphenyl)-4,4-diamine; TcTa, 4,4,4-tris(carbazol-9-yl)triphenylamine; mCP, 1,3-bis(*N*-carbazolyl)benzene; DBFPO, 2,8-bis(diphenylphosphineoxide)-dibenzofuran; Liq, lithium quinolinate.

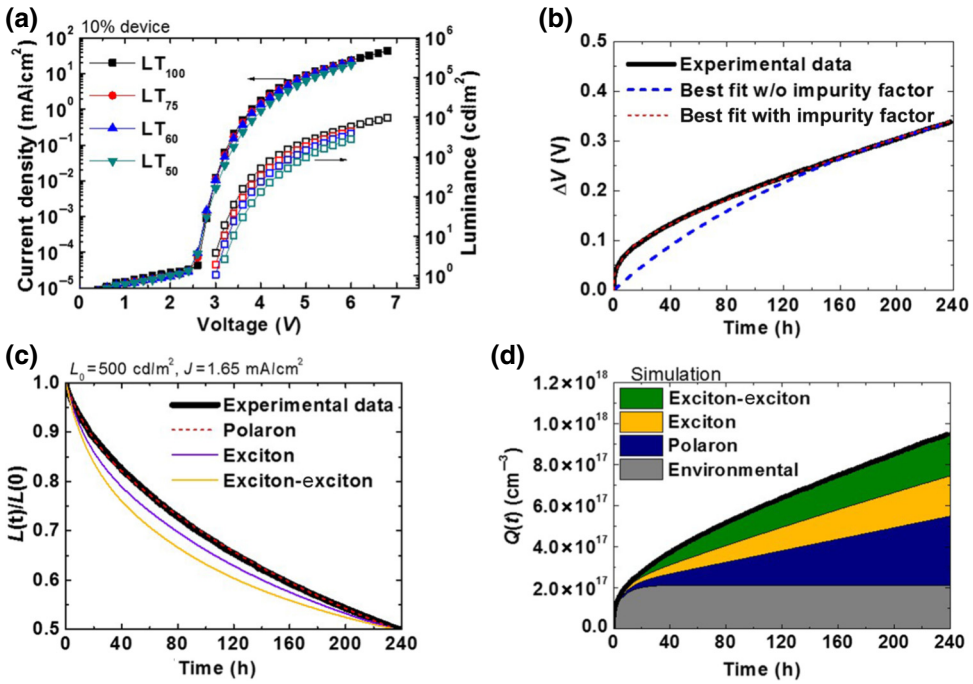

FIG. 3. Analysis of the electrical characteristics of the blue phosphorescent device used in our model over time. (a) J-V-L characteristics of LT_{100} (fresh), LT_{75}, LT_{60}, and LT_{50} devices. (b) Experimental driving-voltage change (black line) fitted by a voltage-rise model, with (red dotted line) and without (blue dashed line) the impurity factor. (c) Luminance and EQE change as a function of time for an initial luminance of 500 cd/m^2 compared with the results of fitting based on different mechanisms, where the impurity effect is included. (d) Quencher densities generated over time by different mechanisms, indicated by differently colored areas.

profiles in the EML are measured experimentally by the sensing-layer method [Fig. 2(f)] to apply the model [22].

The J-V-L characteristics of the aged devices at LT_{100} (fresh), LT_{75}, LT_{60}, and LT_{50} are compared in Fig. 3(a). The current density is reduced upon aging, as expected. Interestingly, however, the charge-injection voltage is maintained the same, without change, in the aged devices as in the pristine device. Figure 3(b) (black line) and Fig. 3(c) (black line) show the rise in the operating voltage (ΔV) and the luminance loss (or EQE loss) over time at a constant current density of $J = 1.65$ mA/cm^2, corresponding to an initial luminance of 500 cd/m^2. It should be noted that the luminance loss is proportional to the efficiency loss because the emission spectra do not change during operation. LT_{50} approaches 238 h, with a voltage rise of 0.34 V.

B. Analysis of driving voltage and calculation of quencher density

The model in Section II assumes that the charge-injection characteristics do not change during operation. The device under investigation indeed satisfies the assumption of stable charge injection during operation, as manifested by the fact that the injection voltage remains the same in the degraded devices as shown in Fig. 3(a), attesting that the built-in potential is remains the same without any interfacial charges, i.e., the charge injection does not change with operation time in the device [5,28]. Therefore, the voltage rise must originate from a reduction of the effective mobility, which can be induced by trapping of charges at degradation products, i.e., quenchers. For instance, the effective mobility in the case of a space-charge-limited current with traps is reduced by a factor of $n/(n + n_t)$, where n and n_t are the densities of free and trapped carriers, respectively.

The generation mechanism and density of the quenchers in the EML and charge-transporting layers are determined using the voltage-rise model. In this simulation, we consider five different quencher generation mechanisms: polarons, excitons, exciton-polaron interactions, exciton-exciton interactions, and impurities, represented by the rate constants $k_{QF}^{P}p$, $k_{QF}^{E} + k_{QF}^{EP}p$, k_{QF}^{EE}, A_0, and $k_{QF}^{\mathrm{imp}}p$, respectively.

Figure 3(b) shows the results of fitting the experimental voltage change (black line) using the model [Eqs. (2) and (3)] developed in this study. Details of the fitting process are described in Appendix B, and the results are shown in Table I. The voltage increase with time cannot be reproduced well just by considering the polaron, exciton, exciton-polaron, and exciton-exciton interactions (k_{QF}^{P}, $k_{QF}^{E} + k_{QF}^{EP}p$, and k_{QF}^{EE}) without the impurity effect (blue dashed line). In contrast, the experimental data are fitted very well if the impurity factor is included (red dot-dashed line). The impurity effect (A_0 and k_{QF}^{imp}) accounts for the rapid increase in driving voltage in the initial stage, and the defect generation rate is exponentially reduced with time as the impurities are consumed by reaction. To confirm that the fitted line in Fig. 3(b) is the only solution of the model, we examine various fittings by changing the fitting parameters, as shown in Fig. S1 in the Supplemental Material [29]. Figure 3(d) shows the contributions of the different degradation processes to the increase in driving voltage. The quencher densities at LT_{50} generated by polarons, exciton-polaron interaction, exciton-exciton

TABLE I. Quencher-generation rate constants from fit to voltage-rise model.

L_0	Doping concentration (%)	$k_{QF}^{P}p\,(\mathrm{cm^{-3}s^{-1}})$	$k_{QF}^{E}+k_{QF}^{EP}p\,(\mathrm{s^{-1}})$	$k_{QF}^{EE}\,(\mathrm{cm^{3}s^{-1}})$	$k_{QF}^{\mathrm{imp}}p\,(\mathrm{s^{-1}})$,	$A_0\ (\mathrm{cm^{-3}})$
500 cd/m^2	10	1.4×10^{15}	2.5×10^{-1}	8.0×10^{-17}	1.6×10^{-1}	2.1×10^{17}
	20	7.84×10^{14}	1.24×10^{-1}	5.87×10^{-17}	9.1×10^{-2}	1.3×10^{17}

annihilation, and the impurity factor are 3.4×10^{17}, 2.0×10^{17}, 2.1×10^{17}, and 2.1×10^{17} cm^{-3}, respectively. These results show clearly that not just a single mechanism but all of the mechanisms together contribute to the generation of quenchers in the device that affect the driving voltage.

C. Quencher generation rate and mechanism in EML

The parameters in Fig. 1, experimentally determined using the pristine device and the equations in Appendix A, are summarized in Table II. The exciton quenching rates corresponding to the processes 6 and 7 in Fig. 1 are obtained by measuring the decreased PL intensity of the host and the radiative lifetime of the emitter excitons, respectively, in the degraded devices at LT_{75}, LT_{60}, and LT_{50}, and are shown in Figs. 4(a) and 4(b) (see Appendix A and Sec. V). The measured quenching rates of the host and dopant excitons and, therefore, the quencher density in the EML increase linearly with operating time if the energy transfer rates (k_{ET}^{DQ}, k_{ET}^{HQ}) are assumed to be constant. These results indicate that the quenchers in the EML are generated by polarons, because the polaron density is kept constant during operation. The exciton-mediated processes (exciton, exciton-polaron, and exciton-exciton) are discarded as origins of quencher generation because the exciton density decreases over time in the EML (Appendix C). The exciton-mediated processes are effective outside the EML, where the quencher generation rate is reduced with operation time. Polaron-induced quencher generation in the EML is supported by the observation that the lifetime acceleration factor (n) [30–32] is close to 1, as shown in Fig. 4(c), where n is the acceleration factor defined in the empirical relationship between the initial luminescence L_0 (at a time equal to 0) and the lifetime of a device shown in Eq. (4):

$$L_0^n \times \mathrm{LT}_x = \mathrm{const.} \tag{4}$$

The EQEs are almost constant from 500 to 3000 cd/m^2 in the device, and so the initial luminance is linearly proportional to the current (polaron) density. Therefore, LT_{50} (or the quencher density) is linearly proportional to the current density or L_0, resulting in $n=1$. If the degradation was induced by exciton-polaron or exciton-exciton mechanisms, n would be greater than 1 and close to 2 because the exciton density and current density must be increased by the same ratio; in other words, the quencher generation rate must be proportional to the square of L_0, so that $n=2$. If the quenchers are generated by excitons, n must be lower than 1.

TABLE II. Experimentally measured parameters used for device simulation.

Parameter	Symbol	Value
Effective radiative decay rate of dopants	Fk_r^D	6.8×10^5 s
Nonradiative decay rate of dopants	$k_{\mathrm{nr,int}}^D$	9.2×10^4 s
Radiative decay rate of host	k_r^H	1.6×10^7 s
Nonradiative decay rate of host	$k_{\mathrm{nr,int}}^H$	1×10^8 s
Host-to-dopant energy transfer rate	k_{ET}^{HD}	6×10^{10} s
Recombination rate in host	k_{rec}^H	4×10^{20} cm^{-3} s^{-1}
Recombination rate at dopants	k_{rec}^D	1.5×10^{20} cm^{-3} s^{-1}
Ratio of exciton formation in host[a] (optical excitation at 337 nm)	α_{PL}	0.91
Ratio of exciton formation in host[b] (electrical excitation)	α_{EL}	0.7
Electron mobility in EML	μ_n	2×10^{-9} cm^2/V s
Hole mobility in EML	μ_h	5×10^{-8} cm^2/V s
Electron density[c]	n	3×10^{17} cm^{-3}
Hole density[c]	p	5×10^{16} cm^{-3}
Trapped hole density[c]	p_t	5×10^{17} cm^{-3}
Width of emission zone[d]	L	15 nm
Relative permittivity	ε	3.5

[a]Calculated from ratio of absorption coefficients.
[b]Calculated from ratio of recombination rates in host and at dopants in the case of hole traps.
[c]Assumed based on the drift-diffusion simulation.
[d]Measured by the sensing-layer method.

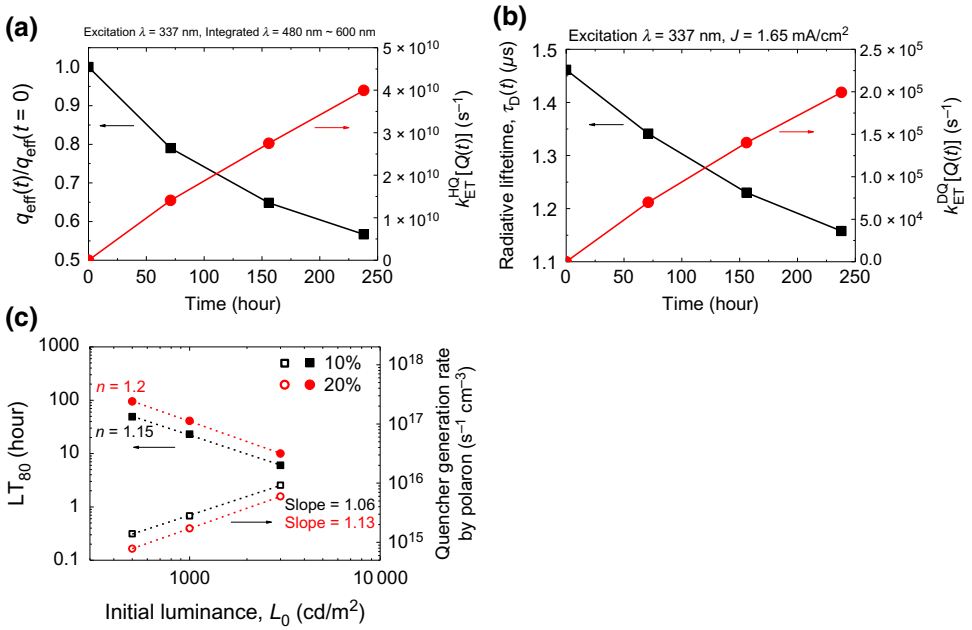

FIG. 4. Exciton quenching rates due to quenchers. (a) Quenching rate of host excitons through energy transfer from host excitons to quenchers (red circles) obtained from the reduced $q_{eff}(t)$ (black squares) and the integrated PL intensity after degradation of the device. (b) Quenching rate of dopant excitons through energy transfer from dopants to quenchers (red circles) extracted from the measured exciton lifetime (black squares) using transient PL data. (c) Operation time LT_{80} (left scale, closed symbols) and quencher generation rate in the EML (right scale, open symbols) under various initial luminance conditions.

D. Quencher generation rate and mechanisms in transporting layers

Of the total number of quenchers, we consider that the polaron-induced quenchers and 20% of the impurity quenchers (there is 30 nm of EML compared with a total 140 nm thickness of the device) are generated in the EML, as discussed in the previous section. Therefore, a Q of 3.8×10^{17} cm^{-3} is present in the EML, out of a total Q of 9.5×10^{17} cm^{-3}, at LT_{50}. The quenchers from exciton interactions analyzed in Fig. 3(d) and 80% of the impurity quenchers are then generated outside the EML. In our device structure, holes are likely to be accumulated at the NPB/TcTa and TcTa/mCBP-CN interfaces due to the energy barriers. Electrons are also likely to leak to the hole-transporting layer (HTL), as inferred from the low energy barrier and the large exciton density near the HTL [Fig. 2(f)]. In addition, the excitons at the interface between the EML and the electron-transporting layer (ETL) and in the ETL can generate quenchers by exciton-polaron (involving both anions and cations) and exciton-exciton interactions due to the high density of polarons. Therefore, exciton-polaron and exciton-exciton interactions can result in the formation of quenchers in the transporting layers along with a portion of the impurity quenchers, thus influencing the driving voltage but not the luminance.

E. Prediction and analysis of the efficiency loss of blue PhOLEDs

With the model, we can predict the EQE and luminance as functions of time and quencher density using the measured rate constants summarized in Table II and Figs. 4(a) and 4(b). We assume that the out-coupling efficiency [$\eta_{out}(t)$] does not change during degradation, because the change in the exciton distribution in the EML is negligible, as deduced from the EL spectra, which remain the same during electrical aging [Fig. 2(e)]. Figure 3(c) shows a comparison of the experimental data (black line) with the theoretical predictions based on different degradation mechanisms. The red dashed line, considering polaron-induced quencher formation in the EML as the degradation mechanism along with the impurity effect, shows excellent agreement with the experimental data compared with assuming mechanisms based on excitons or on exciton-polaron (violet) or exciton-exciton (yellow) interactions. Figure 5(a) shows the EQE loss over time (blue area) together with the loss of exciton formation efficiency (green area) and the effective quantum efficiency (yellow area), calculated using $Q(t)$ in the EML and Eq. (1). The symbols represent experimental values from fresh, LT_{75}, LT_{60}, and LT_{50} devices. The experimental values match perfectly with the calculations (black lines). The excellent match between the simulation and experimental data clearly demonstrates the validity of the model for describing the degradation process of OLEDs. The exciton formation efficiency decreases from 0.92 to 0.81 (88%) at LT_{50}, and the effective quantum efficiency decreases from 0.84 to 0.49 (58%) at LT_{50}, with a Q_{EML} of 3.8×10^{17} cm^{-3}.

F. Prediction of luminance loss at different stress currents

To demonstrate the validity and the predictive power of the model once more, degradation experiments are performed on 10%-doped devices at different initial luminances $L_0 = 1000$ and 3000 cd/m^2, two times and six

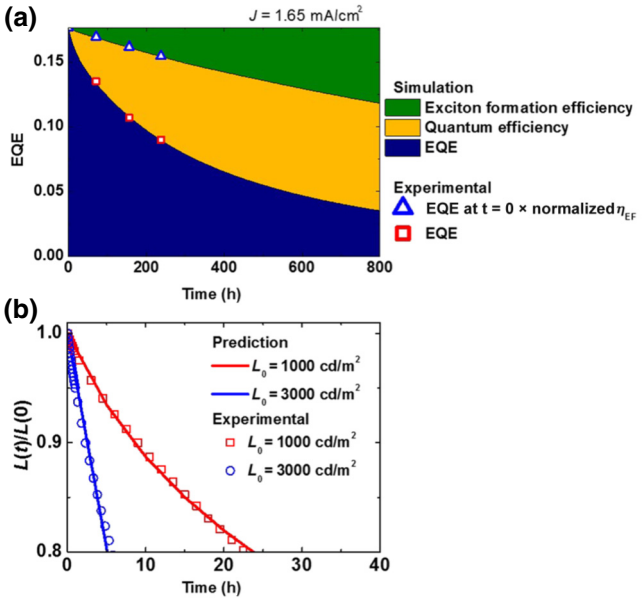

FIG. 5. (a) Contributions of the reduced exciton formation efficiency (green) and the reduced quantum efficiency (yellow area) to EQE loss compared with experimental data (symbols) extracted from LT_{100} (fresh), LT_{75}, LT_{60}, and LT_{50} devices. (b) Prediction of luminance loss at different stress currents corresponding to $L_0 = 1000$ cd/m^2 (red) and 3000 cd/m^2 (blue) using the parameters extracted for $L_0 = 500$ cd/m^2 compared with the experimental data, showing that the model predicts the luminance losses very well.

times higher than the previous value, to check if their degradation characteristics can be predicted using the same set of parameters. The results are shown in Fig. 5(b) for the luminance loss, where the experimental data are predicted very well using the parameters extracted for $L_0 = 500$ cd/m^2, clearly demonstrating the validity and predictive power of the model.

G. A more stable blue PhOLED

The above analysis clearly shows that the luminance degradation in the device is mediated by polarons. Based on this analysis, we increase the doping concentration of emitters in the device to 20% to reduce the quencher formation rate in the EML or to increase the device lifetime. Assuming that the trapped charge density is constant in the 10%- and 20%-doped devices, the charge density per dopant molecule is decreased by one half in the 20%-doped device, with the expectation of doubling the lifetime. The *J-V-L* characteristics, the EQE (with a maximum of 18.3%), the emission spectrum, and the recombination zone of the 20%-doped device are almost the same as for the 10%-doped device, as displayed in Figs. 6(a), 6(b), and 2(f), indicating that the charge-transport properties in the EML do not change much with doping concentration in the device. The injection voltages are maintained at the same value so that the charge-injection characteristics do not change with time either, as shown in Fig. 6(c). As expected, however, the lifetime of the 20%-doped device is two times longer, with an LT_{50} of 431 h for an initial luminance of 500 cd/m^2 as shown in Fig. 6(d). This is the highest reported value of the lifetime up to now for a blue phosphorescent OLED with a CIE y coordinate less than 0.25. An analysis of the degradation mechanisms of the 20%-doped device is shown in Fig. 7. The quencher density in the EML of the 20%-doped device also increases

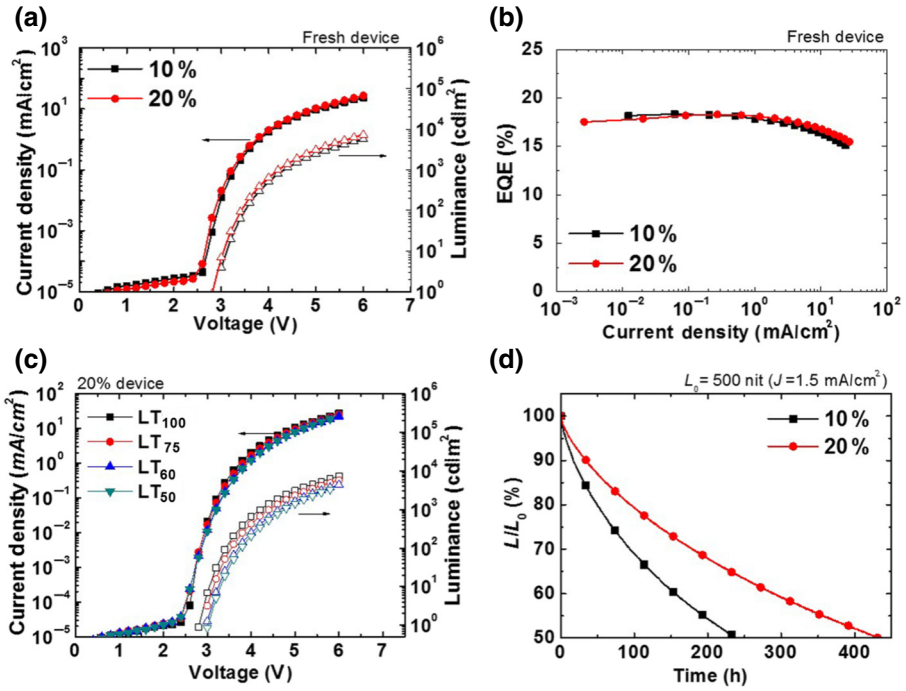

FIG. 6. Electrical characteristics of 10%- and 20%-doped devices. (a) *J-V-L* characteristics of pristine devices. (b) EQE as a function of current density for pristine devices. (c) *J-V-L* characteristics of 20%-doped LT_{100}, LT_{75}, LT_{60}, and LT_{50} devices. (d) Luminance change as a function of time for an initial luminance of 500 cd/m^2. The lifetime of the 20%-doped device is twice as long, with an LT_{50} of 431 h for an initial luminance of 500 cd/m^2.

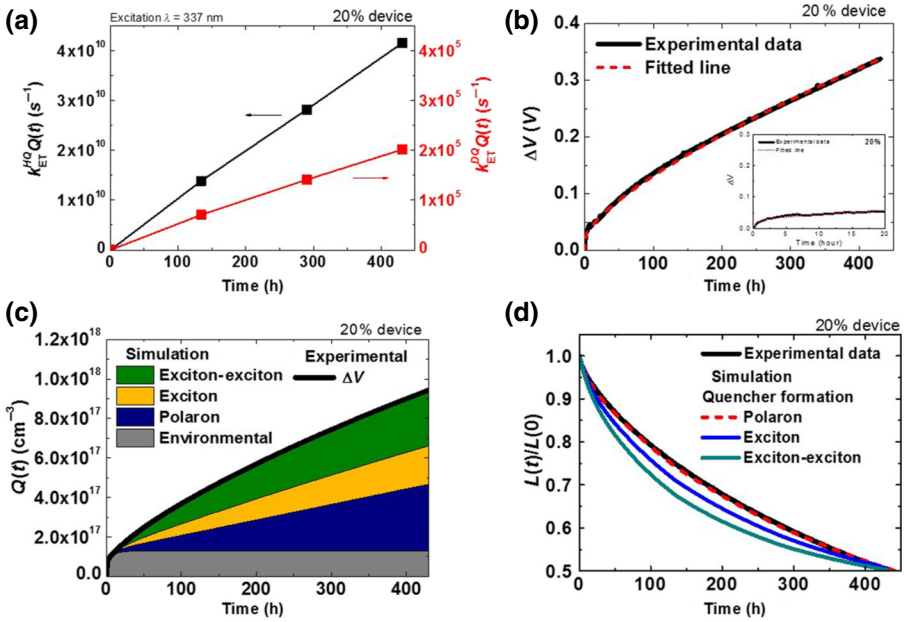

FIG. 7. Analysis results for 20%-doped device. (a) Exciton quenching rate of 20%-doped device. (b) Fitting results of voltage-rise model. (c) Quencher generation rate and density. (d) Prediction of luminance-loss model of the exciton quenching rate in the 20%-doped device.

linearly with operating time, indicating that the quenchers in the EML of the 20%-doped device are generated by polarons as in the 10%-doped device [Fig. 7(a)]. The variations of ΔV, $Q(t)$, and the luminance over time of the 20%-doped device are almost same as for the 10%-doped device, as shown in Figs. 7(b)–7(d), respectively, but the lifetime is doubled due to the quencher formation rate being reduced by one half compared with the rate for the 10%-doped device, as shown in Table I.

H. Quencher analysis by DESI-MS imaging

The above analysis shows that degradation takes place not only in the EML but also in the transporting layers. Polarons and impurities play a major role in degradation in the EML, and other exciton, exciton-polaron, and exciton-exciton interactions degrade the transporting layers. Desorption electrospray ionization mass spectrometry (DESI-MS) of the blue devices is performed to confirm the degradation of the materials. The experimental details of the DESI-MS studies are described in Sec. V. Figure 8(a) shows DESI-MS images of fresh and aged (LT_{10}) devices with 10% Ir dopant. The densities of the dopant ($m/z = 1007.2$), TcTa (HTL, $m/z = 741.3$), and DBFPO (ETL, $m/z = 569.1$) of the aged devices are decreased, while the densities of the host (mCBP-CN, $m/z = 510.2$) and mCP ($m/z = 409.2$) remain similar after degradation. New products with $m/z = 937.3$ and

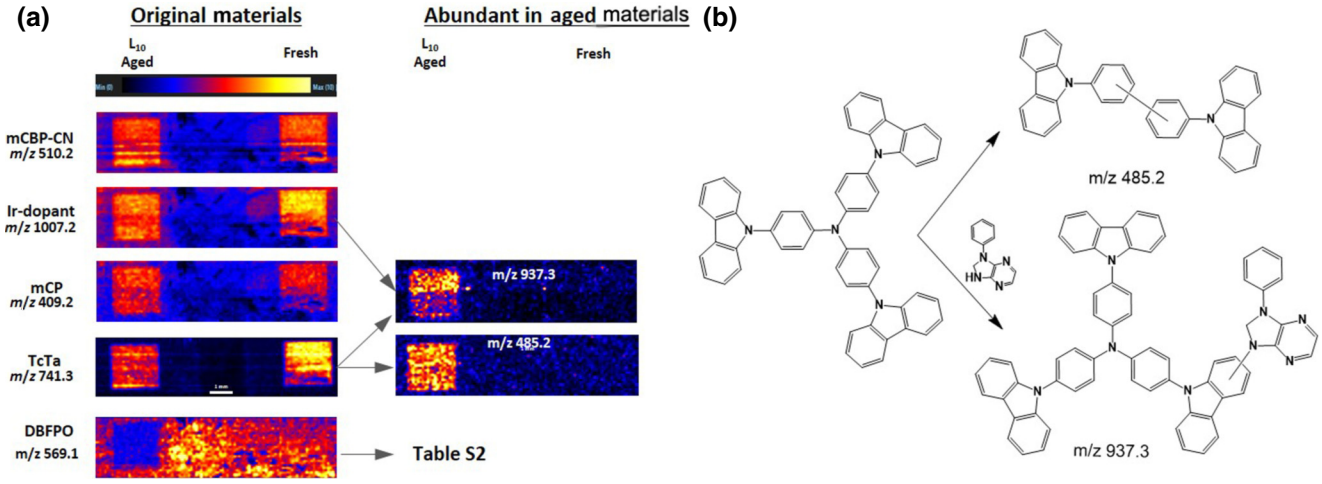

FIG. 8. DESI-MS of electrically degraded device. (a) DESI-MS images of host, dopant, mCP, TcTa, and DBFPO (left column) and of degradation products (right column), and (b) tentative molecular structures and possible reaction pathways to form products with $m/z = 485.2$ and 937.3. The intensities of the colors represent the relative amounts of the materials.

485.2 are observed only in the aged device, as shown in Fig. S3 in the Supplemental Material [29]. Figure 8(b) shows the possible origins of the new products (with $m/z = 485.2$), which may be TcTa molecular fragments generated by dissociation of C—N bonds. The new product with $m/z = 937.3$ could be produced by fragmentation of an Ir-dopant ligand and a TcTa molecule. There is no direct evidence of an Ir-containing fragment present only in an aged pixel with the unique isotope pattern of Ir. Nevertheless, the mass density normalized by that of fresh pixels in the 10%- and 20%-Ir-doped devices (see Fig. S4 in the Supplemental Material [29]) also show decreases in the Ir dopant and TcTa after operation. Other degradation products with m/z values of 369.1, 493.1, 535.2, 585.1, 645.2, 1528.5, 1607.6, 1612.5, and 1624.6 are also found, and the potential molecular structures of these products are listed in Table S1 in the Supplemental Material [29]. Therefore, the results support the inference from the analysis that the dopant is degraded in the EML, and the HTL and ETL are also degraded, as mentioned in previous sections. However, this mass analysis does not give information about the degradation mechanisms of each layer.

IV. CONCLUSION

We present a comprehensive model describing the degradation of OLEDs considering all possible degradation mechanisms, i.e., polarons, excitons, exciton-polaron interactions, exciton-exciton interactions, and impurity effects, in an equation. The degradation process is correlated with the formation of quenchers in the model. Therefore, the model allows us to identify the origin, density, and location of the quenchers using the rise of the operation voltage, the EQE loss, and some independent experiments. Moreover, the variation of the exciton formation efficiency and the EQE during degradation are obtained without any fitting parameters. We apply the model to analyze the degradation process of a highly efficient stable blue phosphorescent OLED, and the results indicate that the model describes the degradation processes of the operation voltage and the EQE under different stresses very well. The analysis suggests that the quenchers are generated not by a single mechanism but by all of the mechanisms outlined above. Interestingly, however, the quenchers in the EML are generated mainly due to degradation of the dopant by polarons and impurities. The analysis indicates that we can increase the lifetime of the device by a factor of 2 by increasing the doping ratio to reduce the polaron density per dopant molecule by a half, and achieve a high efficiency (18% EQE) with the highest value of LT_{50} for blue phosphorescent OLEDs with a CIE y coordinate below 0.25, with a value of 431 h, and with an initial brightness of 500 cd/m^2, using a conventional device structure and conventional materials.

V. EXPERIMENTAL DETAILS

A. Materials

All of the layers in the devices are composed of commercially available materials, which are used without any further purification (sublimed grade). mCBP-CN (>99.96%) and Ir dopant (>99.88%) are synthesized according to the method reported previously [9,33] and purified by sublimation at 10^{-6} Torr. The purity of the materials is determined by high-performance liquid chromatography analysis (Alliance e2695, Waters Corporation, Milford, MA).

B. Device fabrication and characterization

Blue PhOLED devices are fabricated to analyze their performance quantitatively, with the structure ITO (150 nm)/HATCN(10 nm)/NPB(50 nm)/TcTa(5 nm)/mCP (5 nm)/mCBP-CN:Ir dopant(10 wt%, 20 wt%, 30 nm)/DBFPO(10 nm)/DBFPO:Liq(1:1, 30 nm)/Liq(1 nm)/Al (100 nm). The organic, Liq, and metal layers are deposited sequentially on precleaned ITO glass substrates (acetone, isopropanol, deionized water, and UV-ozone treatment) using a thermal evaporation system at a pressure less than 2.0×10^{-7} Torr. The deposition rates of the organic and metal layers are controlled independently from 0.1 to 1 nm s^{-1}, while Liq is deposited at a rate of 0.01 nm s^{-1}. The devices are encapsulated in a nitrogen-filled glove box prior to the measurements. The current-density–voltage–luminance (J-V-L) characteristics and the EL spectra are measured using a programmable source meter (Keithley 2400, active area of devices 4 mm^2) and a spectrophotometer (Photo Research Spectrascan PR650). The EQEs are estimated under the assumption of a Lambertian emission pattern. The lifetime measurements (LT_{50}) of the devices are performed in constant-current mode in a temperature-controlled chamber (at 25 °C). All organic films for optical and electrical characterization are thermally deposited onto quartz or ITO substrates.

C. Photophysical characterization

The transient PL decays and PL spectra of the films and devices are analyzed using a N_2 laser (337 nm) (Usho Optical Systems Co., Osaka, Japan) and a streak-camera system (C10627, Hamamatsu Photonics, Shizuoka, Japan). The electrically pumped transient PL measurements are performed by combining and synchronizing quasi-steady-state electrical pulses (pulse width 200 μs, repetition rate 20 Hz) (DG645, Stanford Research Systems, Sunnyvale, CA), with the transient PL system excited at the middle of the voltage pulses [23].

D. Exciton quenching rate in EML

The radiative lifetime of the dopants at a constant current density of $J = 1.65$ mA/cm^2 is measured by transient

PL of the dopant emission as a function of time in fresh and degraded devices using a streak-camera system, and decreases from 1.46 μs at $t = 0$ to 1.16 μs at LT_{50} (238 h), as shown in Fig. 4(b). The additional nonradiative decay rates originating from energy transfer from the dopant excitons to the quenchers, $k_{ET}^{DQ}Q(t)_{EML}$ (process 7 in Fig. 1 and Appendix A), can be extracted from the exciton lifetimes and increase linearly to 2×10^5 s^{-1} at LT_{50}, as shown in Fig. 4(b). The PL intensities of the dopant emission in the fresh and aged devices are measured, and are also shown to decrease gradually to 57% of that of the fresh device at LT_{50} (from 0.88 to 0.5). The reduction in PL intensity originates from two sources, one from the reduced efficiency of energy transfer from host excitons to dopants (process 6 in Fig. 1 and $k_{ET}^{HQ}Q(t)_{EML}$ in Appendix A) and the other from energy transfer from the dopant excitons to quenchers (process 7 in Fig. 1 and $k_{ET}^{DQ}Q(t)_{EML}$ Appendix A), represented by $I_{PL}(t)/I_{PL}(t = 0) = [\eta_{ET}^{HD}(t)/\eta_{ET}^{HD}(t = 0)] \times [q_{eff}(t)/q_{eff}(t = 0)]$. By combining the quantum efficiency of the dopants obtained by transient PL measurements [Fig. 4(b)] and the quantum efficiency of the EML measured by the reduced PL intensity [Fig. 4(a)], we obtain the energy transfer rate from the host excitons to the quenchers using the equation for $k_{ET}^{HQ}Q(t)_{EML}$ in Appendix A. Figure 4(a) (right scale) shows the energy transfer rate from the host excitons to the quenchers over time, which increases almost linearly to 4×10^{10} s^{-1} at LT_{50}.

E. Quencher analysis

DESI-MS is performed to confirm the degradation products of an electrically degraded blue PhOLED device. Laser desorption ionization is a commonly used technique for analyzing molecular fragmentation. However, there is a limitation on ionizing the electron-transporting materials in our system (see Fig. S2 in the Supplemental Material [29]). The DESI-MS imaging method has been widely used in biotechnology [34,35], but has not been applied to organic electronics. All MS experiments are performed using a mass spectrometer (Synapt G2-Si, Waters Corp., Milford, MA) with a second-generation two-dimensional DESI ion source (Waters Corp.). The samples are placed on a three-dimensional moving stage using double-sided tape and analyzed by DESI-MS in positive-ion mode. Typical instrumental parameters used are 5 kV capillary voltage and 150 °C source temperature. An acetonitrile:water (90:10) solution is used as the spray solvent and is delivered at a flow rate of 1 μl/min. Leucine enkephalin (0.2 ng/μl) is added to the solution as a lock-spray solution. Mass spectra are acquired as full scans in positive mode over the mass range from $m/z = 200$ to $m/z = 1700$. The sprayer-to-surface distance is 1.0–1.5 mm, the sprayer-to-inlet distance is 3–5 mm, and the incident spray is set at 60°. To acquire DESI-MS images, the samples are scanned in horizontal rows separated by 100-μm vertical steps until the specified area of the sample is analyzed. The lines are scanned at a constant velocity of 100 m/s, and the scan time is set to 0.985 s. A spatial resolution (pixel size) in the range of 100 μm × 100 μm is achieved under these conditions. The scan area is defined to be 10 mm in length and 3 mm in width, covering fresh and aged pixels simultaneously for quantitative and qualitative analyses. The data are acquired and processed using the Masslynx 4.0 and HDI 1.4 software packages (Waters Corp.). Multivariate analysis is performed using the Progenesis QI 2.4 software package (Waters Corp.), defining four regions of interest in each active area. An ultrahigh-resolution mass spectrometer (MALDI solariX FT-ICR 9.4 T, Bruker, Karlsruhe, Germany) is used for the analysis. The mass spectrometer is operated in positive-ion mode with a resolution of 400 000 at $m/z = 200$. Two thousand laser shots (at 2 kHz), via a Bruker proprietary Smartbeam II MALDI source, are automatically acquired for each spectrum.

ACKNOWLEDGMENTS

We thank Sangmi Oh from Waters Korea for the DESI-MS measurements. This work was supported by the Industrial Strategic Technology Development Program (Grant No. 10079671) funded by the Ministry of Trade, Industry, & Energy (MOTIE, Korea), and the Samsung Advanced Institute of Technology, Samsung Electronics Co., Ltd.

APPENDIX A: METHODS TO DETERMINE THE PARAMETERS IN EQUATION 1

(1) k_{rec}^{H} ($cm^{-3}s^{-1}$). The Langevin recombination rate at host molecules, which is expressed as follows:

$$k_{rec}^{H} = r_L = \frac{e(\mu_n + \mu_p)}{\varepsilon\varepsilon_0} np,$$

where e is the unit charge, μ_n and μ_p are the electron and hole mobilities in the EML, ε is the relative dielectric constant, and ε_0 is the vacuum permittivity. n and p are the electron and hole densities in the EML, which are simulated using the drift-diffusion model [36]. μ_n and μ_p are measured using electron- and hole-only devices, respectively, as described in our previous studies [36,37].

(2) k_{rec}^{D} ($cm^{-3}s^{-1}$). The trap-assisted recombination rate at dopant molecules, which is expressed as

$$k_{rec(h)}^{D} = r_T = \frac{e\mu_n}{\varepsilon\varepsilon_0} np_t$$

if the dopant molecules behave as hole traps, or

$$k_{rec(e)}^{D} = r_T = \frac{e\mu_p}{\varepsilon\varepsilon_0} pn_t$$

if the dopant molecules behave as electron traps. p_t and n_t in the equation are the trapped hole and electron densities, which are simulated using the drift-diffusion model [36].

(3) k_{ET}^{HD} (s^{-1}). The energy transfer rate from host excitons to dopants, which is expressed as

$$k_{\mathrm{ET}}^{HD} = \frac{1}{\tau_{\mathrm{EML}}^{0}} - \frac{1}{\tau_{H}^{0}} = (k_r^H + k_{\mathrm{nr}}^H + k_{\mathrm{ET}}^{HD}) - (k_r^H + k_{\mathrm{nr}}^H),$$

where τ_{EML}^{0} and τ_H^0 are the exciton lifetimes of the host molecules in the doped host film and in the pristine host film without doping, respectively, and are measured using the transient PL of the host emission of the films. k_r^H and k_{nr}^H are the radiative and nonradiative decay rates, respectively, of the host emission in the film, and are related to the lifetime of the host emission in the pristine host film without doping as follows:

$$\tau_H^0 = \frac{1}{k_r^H + k_{\mathrm{nr,int}}^H}.$$

(4) $Fk_r^D + k_{\mathrm{nr,int}}^D$ (s^{-1}). The sum of the radiative and nonradiative decay rates of the dopant excitons in the OLED, which is obtained from the lifetime (τ_D) of the dopant emission using the following equation:

$$\tau_D = \frac{1}{Fk_r^D + k_{\mathrm{nr,int}}^D},$$

where τ_D is measured using the transient PL of the dopant emission in the fresh device.

(5) $k_{\mathrm{ET}}^{HQ}Q(t)_{\mathrm{EML}}$ (s^{-1}). The energy transfer rate from the host molecules to the quenchers in the EML, which is obtained by measuring the energy transfer efficiency from the host to the dopants, and the already measured k_{ET}^{HD} and $k_{\mathrm{ET}}^{HD} + Fk_r^H + k_{\mathrm{nr,int}}^H$ [item (3)] using the following equation:

$$\eta_{\mathrm{ET}}^{HD}(t) = \frac{k_{\mathrm{ET}}^{HD}}{k_{\mathrm{ET}}^{HD} + Fk_r^H + k_{\mathrm{nr,int}}^H + k_{\mathrm{ET}}^{HQ}Q(t)_{\mathrm{EML}}},$$

where $\eta_{\mathrm{ET}}^{HD}(t)$ is the variation of the energy transfer efficiency with operation time, which is measured using the transient PL and the PL intensity of the dopant emission as a function of the operating time for the degraded devices as described in Sec. V.

(6) $k_{\mathrm{ET}}^{DQ}Q(t)_{\mathrm{EML}}$ (s^{-1}). The energy transfer rate from donors to quenchers, which is obtained using the following equation by measuring the lifetime of the dopant excitons in the degraded devices using the transient PL of the dopant emission, and the already measured exciton lifetime of the dopants (τ_D) in the pristine device [item (4)]:

$$k_{\mathrm{ET}}^{DQ}Q(t)_{\mathrm{EML}} = \frac{1}{\tau_D(t)} - \frac{1}{\tau_D}.$$

(7) $k_{\mathrm{rec}(h)}^{Q}$ ($\mathrm{cm}^{-3}\mathrm{s}^{-1}$). The recombination rate at quenchers, which is calculated using the following equations once $Q(t)$ is known, along with the already calculated μ_n, μ_n, n, p. $Q(t)$ is obtained from $V(t)$ as described in Section C:

$$k_{\mathrm{rec}(h)}^{Q} = \frac{e}{\varepsilon\varepsilon_0}\mu_n Q(t)_{\mathrm{EML}}(1-f)n \quad \text{(hole traps)},$$

$$k_{\mathrm{rec}(e)}^{Q} = \frac{e}{\varepsilon\varepsilon_0}\mu_p Q(t)_{\mathrm{EML}} fp \quad \text{(electron traps)}.$$

(8) $\eta_{\mathrm{EF}}(J,t)$. The exciton formation efficiency, which is obtained using the following equation using the exciton recombination rates in the host, at dopants, and at quenchers, which are already calculated in items (1), (2), and (7) [23]:

$$\eta_{\mathrm{EF}}(J,t) = \left[\frac{J_{Cn}(t) - J_{An}(t)}{J}\right]\left[\frac{k_{\mathrm{rec}}^H + k_{\mathrm{rec}}^D}{k_{\mathrm{rec}}^H + k_{\mathrm{rec}}^D + k_{\mathrm{rec}}^Q(t)}\right].$$

(9) $k_{BQ}(J,t)$ (s^{-1}). The biparticle (exciton-exciton and exciton-polaron) quenching rates in degraded devices, which are obtained using the following equation by measuring the change in the exciton lifetime using the electrically pumped transient PL of the dopant emission of the fresh and degraded devices at a current density J [23]:

$$k_{BQ}(J,t) = \frac{1}{\tau_D(J,t)} - \frac{1}{\tau_D(J=0,t)}.$$

(10) α_{EL}. The ratio of host excitons to total excitons (host excitons + dopant excitons) in the EML, which is obtained using the following equation using the k_{rec}^H and k_{rec}^D already calculated in items (1) and (2):

$$\alpha_{\mathrm{EL}} = \frac{k_{\mathrm{rec}}^H}{k_{\mathrm{rec}}^H + k_{\mathrm{rec}}^D}.$$

APPENDIX B: APPLICATION OF VOLTAGE-RISE MODEL

Consider the device structure shown in Fig. 1, where x is measured from the HTL to the ETL. The generation rate of the quencher density can be represented as follows:

$$\frac{dQ(x,t)}{dt} = k_{QF}^{P}p(x,t) + [k_{QF}^{E} + k_{QF}^{EP}p(x,t)]N(x,t) + k_{QF}^{EE}N(x,t)^2 + k_{QF}^{\mathrm{imp}}p(x,t)A(x,t).$$

Therefore, the density of quenchers during constant-current operation is represented as

$$Q(x,t) = k_{QF}^{P} p(x) t + [k_{QF}^{E} + k_{QF}^{EP} p(x)] \int_0^t N(x,t)\, dt + k_{QF}^{EE} \int_0^t N(x,t)^2\, dt + A(x)_0 [1 - \exp(-k_{QF}^{\text{imp}} pt)].$$

The quencher density at position x and time t can be expressed as $Q(x,t) = Q(t)g(x)$ if the polaron, exciton, and impurity distributions do not change over time. The normalized quencher distribution function, $g(x)$, satisfies the condition $\int_0^L g(x)\, dx = 1$, where L is the thickness of the device. If the total exciton density in the device during electrical operation is assumed to be proportional to that in the emitting layer, $\tilde{N}(t)$, the voltage rise over time is represented as follows:

$$\Delta V(t) = \frac{e}{\varepsilon\varepsilon_0} \int_0^L fxQ(x,t)\, dx,$$

$$\Delta V(t) = \frac{e}{\varepsilon\varepsilon_0} f \begin{pmatrix} k_{QF}^{P} p \int_0^L x g_P(x)\, dx \\ + k_{QF}^{E} \int_0^t N(t)\, dt \int_0^L x g_N(x)\, dx \\ + k_{QF}^{EP} p \int_0^t N(t)\, dt \int_0^L x g_{NP}(x)\, dx \\ + k_{QF}^{EE} \int_0^t N(t)^2\, dt \int_0^L x g_{NN}(x)\, dx \\ + A_0 [1 - exp(-k_{En} t)] \int_0^L x g_{En}(x)\, dx \end{pmatrix}.$$

Here, f is the probability of occupation of quenchers by charges, which is assumed to be 1 if the quenchers are deep traps; $g_P(x)$ is the polaron distribution in the device, which can be calculated by a drift-diffusion simulation; and $g_N(x)$ is the exciton distribution in the device. The exciton profile in the EML is obtained by the sensing-layer method. $g_{NP}(x)$ is the overlap of the polaron and exciton profiles in the device. $g_{NN}(x)$ is expressed as the square of the exciton profile in the device. $g_{En}(x)$ is the profile of the initial impurity density in the device. Then, $\Delta V(t)$ under constant current can be expressed as

$$\Delta V(t) = \left\{ C_1 t + C_2 \int_0^t N(t)\, dt + C_3 \int_0^t N(t)^2\, dt + A* [1 - \exp(-C_4 t)] \right\},$$

where

$$C_1 = k_{QF}^{P} p \int_0^L x g_P(x)\, dx,$$

$$C_2 = k_{QF}^{E} \int_0^L x g_N(x)\, dx + k_{QF}^{EP} p \int_0^L x g_{NP}(x)\, dx,$$

$$C_3 = k_{QF}^{EE} \int_0^L x g_{NN}(x)\, dx,$$

$$A* = A_0 \int_0^L x g_{En}(x)\, dx,$$

and

$$C_4 = k_{QF}^{\text{imp}} p$$

Thus, the voltage rise during electrical operation can be fitted with five fitting parameters, representing a polaron-induced mechanism (C_1), an exciton-related first-order reaction (C_2), an exciton-related second-order reaction, (C_3) and the effect of impurities ($A*$ and C_4), using the known exciton density as a function of time.

APPENDIX C: EXCITON DENSITY, *N(t)*

The initial density of excitons, N_0 is represented as

$$N_0 = \eta_{EF,\text{int}} (k_{\text{rec}}^{H} \eta_{\text{ET,int}}^{HD} + k_{\text{rec}}^{D}) \tau_D.$$

The change of the exciton density over time is

$$\frac{dN(t,t')}{dt'} = \eta_{EF}(t)[k_{\text{rec}}^{H} \eta_{\text{ET}}^{HD}(t) + k_{\text{rec}}^{D}] - [k_r^D + k_{\text{nr}}^{D}(t)] N(t,t'),$$

where t is a time in units of hours and t' is a time in units of microseconds.

At steady state, for a short time range (of the order of microseconds),

$$N(t) = \frac{\eta_{EF}(t)[k_{\text{rec}}^{H} \eta_{\text{ET}}^{HD}(t) + k_{\text{rec}}^{D}]}{k_r^D + k_{\text{nr}}^{D}(t)}$$

(in units of $\text{cm}^{-3} = \text{cm}^{-3}\ \text{s}^{-1}/\text{s}^{-1}$). Alternatively, $N(t)$ can be represented as a function of $L(t)$ as follows:

$$N(t) = N_0 \times L(t)/L_0.$$

[1] S.-Y. Kim, W.-I. Jeong, C. Mayr, Y.-S. Park, K.-H. Kim, J.-H. Lee, C.-K. Moon, W. Brütting, and J.-J. Kim, Organic light-emitting diodes with 30% external quantum efficiency based on a horizontally oriented emitter, Adv. Funct. Mater. **23**, 3896 (2013).

[2] K.-H. Kim, J.-L. Liao, S. W. Lee, B. Sim, C.-K. Moon, G.-H. Lee, H. J. Kim, Y. Chi, and J.-J. Kim, Crystal organic light-emitting diodes with perfectly oriented non-doped Pt-based emitting layer, Adv. Mater. **28**, 2526 (2016).

[3] D. H. Ahn, S. W. Kim, H. Lee, I. J. Ko, D. Karthik, J. Y. Lee, and J. H. Kwon, Highly efficient blue thermally activated delayed fluorescence emitters based on symmetrical and rigid oxygen-bridged boron acceptors, Nat. Photonics **13**, 540 (2019).

[4] H. Shin, Y. H. Ha, H.-G. Kim, R. Kim, S.-K. Kwon, Y.-H. Kim, and J.-J. Kim, Controlling horizontal dipole orientation and emission spectrum of Ir complexes by chemical

design of ancillary ligands for efficient deep-blue organic light-emitting diodes, Adv. Mater. **31**, 1808102 (2019).
[5] S. Scholz, D. Kondakov, B. Lussem, and K. Leo, Degradation mechanisms and reactions in organic light-emitting devices, Chem. Rev. **115**, 8449 (2015).
[6] N. C. Giebink, B. W. D'Andrade, M. S. Weaver, P. B. Mackenzie, J. J. Brown, M. E. Thompson, and S. R. Forrest, Intrinsic luminance loss in phosphorescent small-molecule organic light emitting devices due to bimolecular annihilation reactions, J. Appl. Phys. **103**, 044509 (2008).
[7] H. Yamamoto, J. Brooks, M. S. Weaver, J. J. Brown, T. Murakami, and H. Murata, Improved initial drop in operational lifetime of blue phosphorescent organic light emitting device fabricated under ultra high vacuum condition, Appl. Phys. Lett. **99**, 033301 (2011).
[8] J. Lee, C. Jeong, T. Batagoda, C. Coburn, M. E. Thompson, and S. R. Forrest, Hot excited state management for long-lived blue phosphorescent organic light-emitting diodes, Nat. Commun. **8**, 15566 (2017).
[9] S. Kim, H. J. Bae, S. Park, W. Kim, J. Kim, J. S. Kim, Y. Jung, S. Sul, S.-G. Ihn, C. Noh, S. Kim, and Y. You, Degradation of blue-phosphorescent organic light-emitting devices involves exciton-induced generation of polaron pair within emitting layers, Nat. Commun. **9**, 1211 (2018).
[10] P. Heimel, A. Mondal, F. May, W. Kowalsky, C. Lennartz, D. Andrienko, and R. Lovrincic, Unicolored phosphor-sensitized fluorescence for efficient and stable blue OLEDs, Nat. Commun. **9**, 4990 (2018).
[11] N. C. Giebink, B. W. D'Andrade, M. S. Weaver, J. J. Brown, and S. R. Forrest, Direct evidence for degradation of polaron excited states in organic light emitting diodes, J. Appl. Phys. **105**, 124514 (2009).
[12] Q. Wang, B. Sun, and H. Aziz, Exciton-polaron-induced aggregation of wide-bandgap materials and its implication on the electroluminescence stability of phosphorescent organic light-emitting devices, Adv. Funct. Mater. **24**, 2975 (2014).
[13] D. Y. Kondakov, W. C. Lenhart, and W. F. Nichols, Operational degradation of organic light-emitting diodes: Mechanism and identification of chemical products, J. Appl. Phys. **101**, 024512 (2007).
[14] A. S. D. Sandanayaka, T. Matsushima, and C. Adachi, Degradation mechanisms of organic light-emitting diodes based on thermally activated delayed fluorescence molecules, J. Phys. Chem. C **119**, 23845 (2015).
[15] H. Yu, Y. Zhang, Y. J. Cho, and H. Aziz, Exciton-induced degradation of carbazole-based host materials and its role in the electroluminescence spectral changes in phosphorescent organic light emitting devices with electrical aging, ACS Appl. Mater. Interfaces **9**, 14145 (2017).
[16] T. D. Schmidt, L. Jager, Y. Noguchi, H. Ishii, and W. Brutting, Analyzing degradation effects of organic light-emitting diodes via transient optical and electrical measurements, J. Appl. Phys. **117**, 215502 (2015).
[17] K. W. Hershey, J. S. Bangsund, G. Qian, and R. J. Holmes, Decoupling degradation in exciton formation and recombination during lifetime testing of organic light-emitting devices, Appl. Phys. Lett. **111**, 113301 (2017).
[18] J. S. Bangsund, K. W. Hershey, and R. J. Holmes, Isolating degradation mechanisms in mixed emissive layer organic light-emitting devices, ACS Appl. Mater. Interfaces **10**, 5693 (2018).
[19] Q. Niu, C.-J. A. Q. Niu, C.-J. A. H. Wetzlaer, P. W. M. Blom, and N. I. Craciun, Modeling of electrical characteristics of degraded polymer light-emitting diodes, Adv. Electron. Mater. **26**, 1600103 (2016).
[20] M. A. Baldo, C. Adachi, and S. R. Forrest, Transient analysis of organic electrophosphorescence: I. Transient analysis of triplet-triplet annihilation, Phys. Rev. B **62**, 16 (2000).
[21] S. Reineke, K. Walzer, and K. Leo, Triplet-exciton quenching in organic phosphorescent light-emitting diodes with Ir-based emitters, Phys. Rev. B **75**, 125328 (2007).
[22] N. C. Giebink and S. R. Forrest, Quantum efficiency roll-off at high brightness in fluorescent and phosphorescent organic light emitting diodes, Phys. Rev. B **77**, 235215 (2008).
[23] B. Sim, C.-K. Moon, K.-H. Kim, and J.-J. Kim, Quantitative analysis of the efficiency of OLEDs, ACS Appl. Mater. Interfaces **8**, 33010 (2016).
[24] S. Nowy, B. C. Krummacher, J. Frischeisen, N. A. Reinke, and W. Brutting, Light extraction and optical loss mechanisms in organic light-emitting diodes: Influence of the emitter quantum efficiency, J. Appl. Phys. **104**, 123109 (2008).
[25] M. Murgia, R. H. Michel, G. Ruani, W. Gebauer, O. Kapousta, R. Zamboni, and C. Taliani, In-situ characterization of the oxygen induced changes in a UHV grown organic light-emitting diode, Synth. Met. **102**, 1095 (1999).
[26] T. Ikeda, H. Murata, Y. Kinoshita, J. Shike, Y. Ikeda, and M. Kitano, Enhanced stability of organic light-emitting devices fabricated under ultra-high vacuum condition, Chem. Phys. Lett. **426**, 111 (2006).
[27] S.-G. Ihn, N. Lee, S. O. Jeon, M. Sim, H. Kang, Y. Jung, D. H. Huh, Y. M. Son, S. Y. Lee, M. Numata, H. Miyazaki, R. G. Bombarelli, J. A. Iparraguirre, T. Hizel, A. A. Guzik, S. Kim, and S. Lee, An alternative host material for long-lifespan blue organic light-emitting diodes using thermally activated delayed fluorescence, Adv. Sci. **4**, 1600502 (2017).
[28] F. So and D. Kondakov, Degradation mechanisms in small-molecule and polymer organic light-emitting diodes, Adv. Mater. **22**, 3762 (2010).
[29] See the Supplemental Material at http://link.aps.org/supplemental/10.1103/PhysRevApplied.14.024002 for details regarding the characterization of the voltage-rise model and the analysis by DESI-MS.
[30] Y. Sato, S. Ichinosawa, and H. Kanai, Operation characteristics and degradation of organic electroluminescent devices, IEEE J. Sel. Top. Quantum Electron. **4**, 40 (1998).
[31] R. C. Kwong, M. R. Nugent, L. Michalski, T. Ngo, K. Rajan, Y.-J. Tung, M. S. Weaver, T. X. Zhou, M. Hack, M. E. Thompson, S. R. Forrest, and J. J. Brown, High operational stability of electrophosphorescent devices, Appl. Phys. Lett. **81**, 162 (2002).
[32] C. Féry, B. Racine, D. Vaufrey, H. Doyeux, and S. Cina, Physical mechanism responsible for the stretched exponential decay behavior of aging organic light-emitting diodes, Appl. Phys. Lett. **87**, 213502 (2005).
[33] O. Molt, C. Lennartz, G. Wagenblast, E. Fuchs, N. Langer, C. Schidknecht, K. Dormann, S. Watanabe, T. Schaefer, H. Wolleb, T. Marina, F. Duarte, S. Metz, and P. Murer (UDC Ireland Ltd.), Metal complexes comprising

dazabenzmidazolocarbene ligands and the use thereof in OLEDs, US20130032766A1 (2013).

[34] Y. Dong, B. Li, S. Malitsky, I. Rogachev, A. Aharoni, F. Kaftan, A. Svatos, and P. Franceschi, Sample preparation for mass spectrometry imaging of plant tissues:A review, Front. Plant Sci. **7**, 60 (2016).

[35] J. Xu, *et al.*, Panax ginseng genome examination for ginsenoside biosynthesis, Giga Sci. **6**, 11 (2017).

[36] C.-H. Lee, J.-H. Lee, K.-H. Kim, and J.-J. Kim, Unveiling the role of dopant polarity in the recombination and performance of organic light-emitting diodes, Adv. Funct. Mater. **28**, 1800001 (2018).

[37] J.-M. Kim, C.-H. Lee, and J.-J. Kim, Mobility balance in the light-emitting layer governs the polaron accumulation and operational stability of organic light-emitting diodes, Appl. Phys. Lett. **111**, 203301 (2017).